Multiparameter POF Sensing Based on Multimode Interference and Fiber Bragg Grating

Ricardo Oliveira, Thiago H. R. Marques, Lúcia Bilro, Rogério Nogueira, *Member, IEEE, Senior Member, OSA*, and Cristiano M. B. Cordeiro

***Abstract*—We report the fabrication of a multimode interferometer (MMI), based on a multimode polymer optical fiber (POF), sandwiched between two single-mode silica fibers. The POF used in this work is a step-index fiber with core and cladding composed of a cycloolefin polymer (COP) and PMMA, respectively. The low moisture absorption of the COP material and the benefit of having an exposed core for refractive index measurements in MMI devices lead us to perform an etching of the PMMA layer. Additionally, we report the inscription of a Bragg grating in the COP core material of an etched single-mode-multimode-single-mode (SMS) structure. The two fiber structures were simultaneously characterized to strain, temperature, humidity, and refractive index. The ability to detect refractive index by using a POF-based SMS structure is reported for the first time in this paper. Additionally, the capability for dual parameter measurement was discussed using both FBG and SMS structures.**

***Index Terms*—Etching, fiber Bragg grating (FBG), multimode interference (MMI), optical fiber sensor, plastic optical fiber (POF).**

I. Introduction

NOWADAYS, fiber optic sensors have been widely used to detect physical, chemical, and biological parameters. This has been done due to the qualities offered by fiber optic sensors, such as the immunity to electromagnetic noise, light weight, small size and in some cases the ability to multiplex signals [1].

Commonly, silica fibers have been the preferred choice for the production of fiber optic sensors. However, polymer optical fibers (POFs) have been pointed as an alternative to silica fibers, due to the special characteristics that polymers may offer. In fact, when compared with silica, polymers have several advantages such as: negative and much larger thermo-optic coefficient [2]; smaller Young modulus [1], allowing to withstand with high elongation regimes [3], [4]; flexibility in bending; non-brittle nature and biological compatibility [5]. Additionally, polymers are easier to process [2]. These advantages have led the scientific community to develop different fiber optic sensors based on POFs. Among the different polymer materials available, polymethylmethacrylate (PMMA) is the most commonly used for the production of POF [2]. Since this material has the ability to absorb water, POFs can be used as humidity sensors [6]–[8]. Nevertheless, other polymers with good transparency in the visible and near-infrared region have also been employed as the core and cladding materials of multicore; step-index; and also microstructured POFs (mPOFs). Examples of such polymers are: polycarbonate (PC) [9], polystyrene, CYTOP (amorphous fluoropolymer), TOPAS (a cycloolefin copolymer COC) [5], [10] and ZEONEX (a cycloolefin polymer COP) [11], Their attractiveness is related with the high glass transition temperature (145 °C for the PC and, 138 °C for COC and COP [2]); low water absorption ($<0.01\%$ per day) and high chemical resistance for the COC, COP and CYTOP materials [2], [12]. Therefore, POF sensors based on these materials have been reported to withstand at high temperatures [9], [13], [14] and also to be humidity insensitive [10], [13].

Among the different fiber optic sensors technologies, one that is receiving attention in recent years is the fiber modal interferometry, commonly known as MMI (multimode interference). This device comprises a single-mode-multimode-single-mode (SMS) fiber structure and the inherent simple fabrication, low production cost and the high sensitivity and compactness that it can offer, allows the detection of a variety of parameters, such as: strain [15], temperature [16], liquid level [17] and refractive index [18]–[20]. In order to measure the refractive index, the core fiber must be exposed to the environment. This can be done with a multimode fiber (MMF) composed of a single material commonly known as no-core-fiber (NCF) [19], or by simply etching the cladding of a MMF [18], [20].

The inherent advantages of POFs when compared with silica fibers, lead also to the development of SMS structures based on those fibers. Thus a POF device based on multimodal interference (MMI-POF) has already been proposed for large strain measurement [3]. Additionally, the capability to detect strain and temperature in the low loss region of perfluorinated [21] and also partially chlorinated [22] graded index POFs was already subject of study.

Another fiber optic technology that is well known and widely spread in different sensing areas is the fiber Bragg grating (FBG). This technology has already proven its feasibility to detect a variety of parameters, such as strain [23], temperature, curvature, refractive index [24], etc. Moreover, the inscription

Manuscript received August 22, 2016; revised October 5, 2016; accepted November 4, 2016. Date of publication November 8, 2016; date of current version December 12, 2016. This work was supported in part by the FCT-Fundação para a Ciência e Tecnologia through Portuguese national funds by UID/EEA/50008/2013 (project SWAT) and in part by the hiPOF (PTDC/EEI-TEL/7134/2014), Ph.D. Scholarship SFRH/BD/88472/2012, investigator grant IF/01664/2014 and project INITIATE, and in part by the FINEP under the Project 0112039300.

R. Oliveira and R. Nogueira are with the Instituto de Telecomunicações, Aveiro 3810-193, Portugal (e-mail: oliveiraricas@av.it.pt; rnogueira@av.it.pt).

T. H. R. Marques and C. M. B. Cordeiro are with the Instituto de Física "Gleb Watagin", Universidade Estadual de Campinas, Campinas 13083-970, Brazil (e-mail: rosales@ifi.unicamp.br; cmbc@ifi.unicamp.br).

L. Bilro is with the Instituto de Telecomunicações, Aveiro 3810-193, Portugal, and also with the I3N/FSCOSD—Institute of Nanostructures, Nanomodelling and Nanofabrication—Physics Department, University of Aveiro, Aveiro 3810-193, Portugal (e-mail: lucia.bilro@av.it.pt).

Color versions of one or more of the figures in this paper are available online at http://ieeexplore.ieee.org.

Digital Object Identifier 10.1109/JLT.2016.2626793

and characterization of FBGs in different POFs (POFBGs), in the visible and near-infrared region is currently being subject of study. The inscription has been performed essentially by the phase mask technique, either by using a 325 nm continuous UV radiation [7], [9], [13], [25], or by using a 248 nm pulsed UV radiation, where the later has proven to inscribe Bragg gratings in few seconds [26].

In this work we have used a step-index multimode POF, composed of a ZEONEX 480R core and PMMA cladding, to produce an SMS structure and a POFBG capable of measure strain, temperature and refractive index. In order to allow the interaction of the core guided modes with the external environment for the refractive index characterization, the PMMA cladding of the POF was firstly etched. Additionally, the low water absorption characteristic of COP core material permits the development of a humidity insensitive POF sensor. After the etching process, a POFBG was written for the first time in the unclad multimode POF. Additionally, the capability to measure refractive index, using an SMS structure based on POF, is demonstrated for the first time, revealing sensitivities similar to the ones reported for silica SMS structures. Furthermore, the refractive index experimental results of the SMS structure were also compared with the ones obtained theoretically, showing good agreement. Moreover, the sensitivities obtained for the two fiber structures, can be used for simultaneous measurement of two parameters.

II. Operating Principle and Sensor Fabrication

A. Operating Principle

The theoretical concept underlying the MMI can be explained by the self-imaging phenomenon. This occurs when the output light field of a single mode fiber (SMF) enters into a MMF section, exciting higher order modes within the MMF. Interference between these modes will accumulate, giving rise to the formation of replicas in both amplitude and phase of the leading SMF output signal at periodic intervals along the axis of the MMF. The length in which the self-images are formed can be obtained from the restricted symmetric interference condition, given at [27], [28]:

$$L = p\frac{n_{\mathrm{MMF}} D_{\mathrm{MMF}}^2}{\lambda_0} \tag{1}$$

where, n_{MMF} and D_{MMF} are respectively the effective refractive index and diameter of the MMF, λ_0 is the free space wavelength and p the self-image number. If the MMF is cleaved at a distance where one of the self-images is being formed, then a well-defined peak will occur at the wavelength λ_0, being this sensitive to the external conditions, such as strain [15], temperature [16], liquid level [17] and refractive index [18]–[20].

B. Multimode POF Etching Process

The MMF used in this work was fabricated at Universidade Estadual de Campinas being a step-index POF composed of ZEONEX 480R and PMMA materials with diameters of 73.5 μm and 446 μm, respectively for the core and cladding.

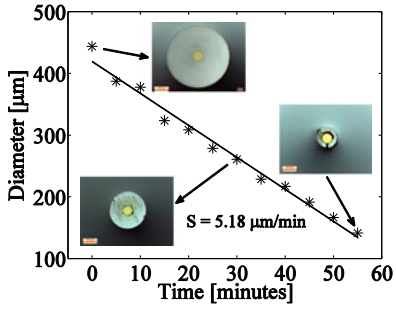

Fig. 1. Evolution of the PMMA etching process, necessary to expose the COP core material.

It is known that PMMA based POFs can be used to sense liquid refractive index [29], however, the sensing mechanism is intrinsically related to the amount of water absorbed by the PMMA. This leads to the swelling of the fiber and to a change in the material refractive index [29]. Moreover, the PMMA water uptake can be a time consumption process which can take several tens of minutes, depending on the diameter of the POF [6]–[8]. On the other hand, COP material has low water absorption as well as excellent chemical resistance (e.g. alcohol, acetone [2]). Nevertheless, the mechanism behind the detection of external refractive index in silica optical fiber sensors relies on the interaction between guided mode(s) end external environment. In fiber based MMIs, this is usually done by using either a solid core fiber [19], or by etching the cladding layer of an MMF [18].

To produce a POF based SMS structure capable of measuring external refractive index, the fiber cladding needs to be removed. Thus, acetone was used to etch the PMMA cladding layer. Nevertheless, the COP core material is known to have chemical resistance to acetone [30], but our preliminary tests showed that long exposure times to acetone gives rise to formation of surface cracks, which inherently affects the guiding properties of the POF. Therefore, the etching rate was monitored during time. The optical fiber overall diameter evolution can be seen in Fig. 1.

From the inset pictures presented in Fig. 1, it is clearly visible that the PMMA cladding surrounding the COP core material reduces its diameter with etching time. The etching rate was estimated through a linear fit to be 5.18 μm/min. Thus, to completely remove the PMMA cladding layer a period of about 70 minutes is needed.

C. Fiber Bragg Grating Inscription

Fiber Bragg Gratings are very attractive due to the easy integration in optical components. When recorded in POFs, several advantages can be obtained when compared to their silica counterparts. Additionally, combining FBGs with other fiber optic technologies brings the opportunity to simultaneously detect different parameters. Therefore, we decide to inscribe a POFBG in the etched-POF. Prior to the inscription process, the fiber was annealed at 80 °C during 24 hours in order to remove any residual stresses created during the fabrication process. The POFBG was written at 1550 nm region with a KrF excimer laser through the methodology described before [26], [31], which demonstrated

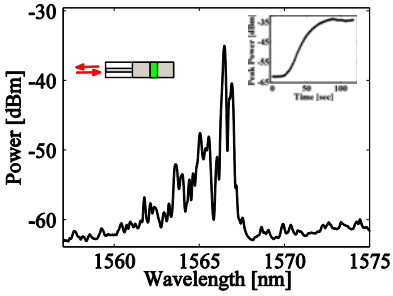

Fig. 2. POFBG spectra collected for an etched multimode POF with a phase mask pitch of 1033 nm. The inset on the left shows the measurement scheme used (reflection), where the inset on the right shows the peak power evolution during the inscription process.

to be the fastest method to inscribe high quality POFBGs. The laser repetition rate was set to 5 Hz and the energy set to its minimum (3 mJ). After the beam exit, an attenuator is used to decrease the energy to 0.5 mJ, avoiding ablative process on the polymer surface. The UV beam is then passed through a cylindrical lens and a slit with 4.5 mm in width shapes the beam onto the phase mask ($\Lambda = 1033$ nm) that is prior to the etched-POF. The grating growth was monitored in reflection through a silica pigtail fiber, cleaved at an APC angle and butt coupled to the etched-POF. The peak growing was seen by an interrogation system (1 pm in resolution), allowing to know when the saturation time is achieved, in order to switch the laser off. After 15 seconds, the POFBG starts to grow and after 80 seconds the POFBG has reached its maximum with a peak to noise level of 25 dB (see Fig. 2).

As can be seen from Fig. 2, the spectrum presents several peaks at around 1565 nm, which are inherently due to the multimode nature of the etched-POF.

D. Numerical Simulations

In order to know the length of the etched-POF needed to produce a peak centered at 1550 nm region, we have employed a two dimensional beam propagation method (BPM). For that, an input silica-SMF with diameter of 8.2 and 125 μm and refractive index at 1550 nm of 1.44615 and 1.43950, respectively for the core and cladding was considered. Regarding the etched-POF, the diameter was 73.5 μm and the refractive index at 1550 nm was 1.51 (extrapolated from the data taken in reference [2]). The simulation area was set to 130 μm in height and 13 mm in length, where the content surrounding the fibers was filled with the refractive index of air ($n = 1$).

The correspondent light field distribution is shown on Fig. 3(a), where a periodical evolution of the light field is observed along the etched-POF's length. The correspondent normalized field amplitude at 1550 nm is also presented (Fig. 3(b)). The first image is located approximately at 5.11 mm from the input fiber tip, being the position of the other images an integer multiple of the first image. Regarding that, the etched-POF should be cleaved at one of these maxima. Hence, in order to have enough length for the splicing process and for the posterior strain characterization test, we choose the 20th image, which corresponds to a length of 10.22 cm.

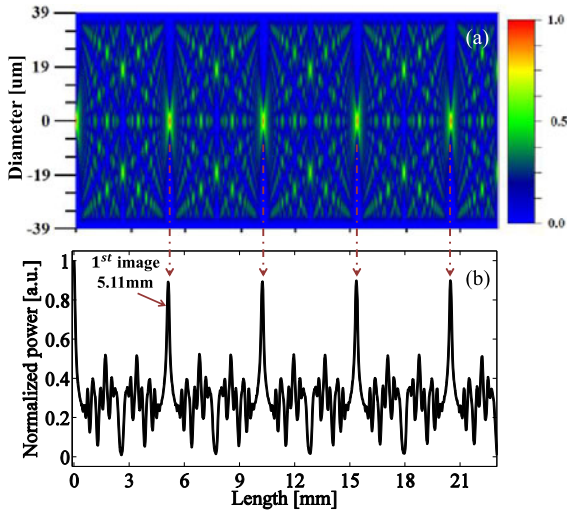

Fig. 3. (a) The light field injected at the left by a silica SMF evolves periodically as it propagates along the fiber core. (b) Power normalized to the input power, along the optical axis of the etched-POF.

E. SMS Structure Assembly

The length of the etched-POF containing the FBG was measured with a digital caliper and the fiber tips were cleaved perpendicularly to the length at both ends with a sharp razor blade with a length of 10 ± 1 mm. Two silica-SMF pigtails were cleaved with PC and APC terminals and were used to splice each terminal of the prepared etched-POF. The APC silica pigtail fiber was used to monitor the reflection signal from the POFBG, allowing thus, the reduction of the background noise. The fibers' alignment (through their centers) was performed through 3D mechanical positioners with the help of two cameras positioned in each orthogonal axis. After that, a drop of an UV curing optical adhesive (Loctite 3525) is carefully placed in each fiber terminal, following up longitudinal alignment and the UV curing process. This particular glue was chosen to give enough strength for the manipulation during the characterization tests (shore hardness D 60), allowing also refractive index matching between the fibers ($n_{glue,\ cured}(589\ nm) = 1.51$). Additionally, the glue can withstand at high temperature range (i.e. -40 to 140 °C), presenting also toughness, durability to moisture exposure and good resistance to alcohols [32]. The whole process, together with the final SMS structure based on the etched-POF can be seen on Fig. 4.

After final assembly of the SMS structure, the fiber was kept straight and the transmission spectrum was taken (see Fig. 5).

As can be seen, the transmission spectrum shown in Fig. 5 presents several peaks and valleys, contrary to the expected (one peak centered at 1550 nm). This result could have three main contributions: the etched-POF could be cleaved with a length different from the predicted by BPM simulation; a possible mismatch between the fibers on the positioning process; and spreading of glue onto the etched-POF tip, which inherently affects the refractive index of the external environment on that region. The peaks/valleys, however, can still be used to measure the external stimuli (ex. peak marked with red dot). In Fig. 5, a small valley around 1565 nm is also observed (next to the peak

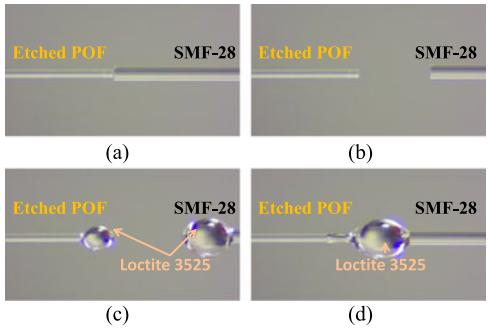

Fig. 4. (a) and (b) Axial alignment between the silica SMF and the etched-POF. (c) Insertion of Loctite 3525 glue at each fiber terminal. (d) Final alignment and curing process by the use of a UV lamp.

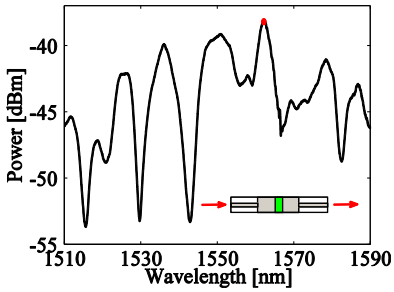

Fig. 5. Transmission power spectrum after the SMS structure based on an etched-POF. The inset shows the measurement scheme used for the signal detection (transmission).

marked with a red dot). This peak is due to the filtering produced by the POFBG. Since it does not present enough peak to noise level, we decide not to use it for the characterizations - instead we have used the reflection signal from the POFBG (Fig. 2).

III. Experimental Setup

A. Strain, Temperature, Humidity and Refractive Index Characterization

For the strain characterization, the fiber splices were fixed with glue to a static and to a linear stage. The distance between the stages where the glue was inserted was 10 cm and the SMS structure was kept straight to avoid curvature effects on the SMS structure. The strain was made in steps of 1 mε, in a total extension of 15 mε (1.5%). The characterization was implemented in a climatic chamber (Angelantoni CH340), keeping the temperature at 25.0 $\pm$ 0.3 °C and the relative humidity at 80 $\pm$ 3%.

Regarding the temperature characterization, the fiber was kept straight and the relative humidity was set to 80%. Since the maximum operation temperature of ZEONEX 480R is between 100 to 110 °C [30], we decide to run the temperature test from 25 to a maximum of 105 °C. The temperature was swept in steps of 5 °C, giving 30 minutes of stabilization before signal acquisition.

The low water absorption provided by the COP material offers advantages regarding the development of POF sensors insensitive to humidity. In order to know the POFBG and SMS wavelength stability due the water absorption, a humidity test was performed with the fiber straight and with a constant temperature of 25 °C. The relative humidity was swept from 30% to 90% in steps of 10%, giving 3 hours for each step, allowing enough time for the uptake of water by the COP polymer.

Concerning the refractive index test, the fiber was left straight and the temperature was kept at 25 °C. In this test, a "U" shape liquid container was inserted below the etched-POF and between the mechanical stages used for the strain test. This container was glued at the edges, preventing leakage of the liquid solutions. Five different solutions of water/isopropyl alcohol were prepared and the refractive index was measured at 589 nm and 25 °C, using an Abbemat 200 refractometer with resolution of 1×10^{-6}.

In order to observe both POFBG and SMS spectral responses, an interrogator system (Micron Optics 125-500) was used to measure the reflection signal from the FBG as well as the transmission signal from the SMS structure. For that, one of the interrogator channels works as input/output, injecting light into the sensor and detecting the FBG reflection signal. The light that passes through the SMS structure goes to a fiber isolator and it is detected at the second interrogator channel. Here, the isolator allows the second channel to function only as an input. It is known that the spectral position of the MMI peaks can be dependent on the polarization state of light [33]. Thus, in order to avoid inherent errors associated with that, we did not change the polarization state of light during the measurement experiments.

IV. Results and Discussion

The strain tests (at constant temperature) can be observed in Fig. 6(a) (POFBG signal in reflection) and Fig. 6(b) (SMS structure signal in transmission). When the strain is increased, the wavelength peak (marked with a red diamond) revealed positive and negative shifts for the POFBG and SMS structure respectively. These results are summarized in Fig. 7(a). From that, a linear evolution of the wavelength shifts for the load and unload cases is observed, showing no hysteresis for both fiber structures. By adjusting linear fits to the data points, a POFBG sensitivity of 1.51 ± 0.01 pm/$\mu\varepsilon$ for both loading and unloading cases, with R-square values of 0.999 is found. The sensitivities are similar to the ones found for step-index and microstructured POFs [8], [13], [25]. Regarding the SMS wavelength shifts, the applied linear regression model has produced sensitivities of -3.03 ± 0.01 pm/$\mu\varepsilon$ and -2.99 ± 0.01 pm/$\mu\varepsilon$ respectively for the loading and unloading cases, with R-square values of 0.999. When compared with literature for SMS structures based on POF, it can be seen that the absolute value is quite similar to the ones presented for PMMA [3] and partially chlorinated [22] based POFs. Nevertheless, the value is still lower than the one obtained for a perfluorinated based POF (111.8 pm/$\mu\varepsilon$) [21].

Concerning the temperature tests, when the temperature is increased a blue-shift of the POFBG reflection spectra and a red-shift of the SMS transmission spectra occurs – see blue dots in Fig 6(a) and (c). The measurement of the peak wavelength shift of both POFBG reflection and SMS transmission spectra, for the increasing and decreasing temperature, can be seen in Fig. 7(a). The results reveal linear tendency, however, some

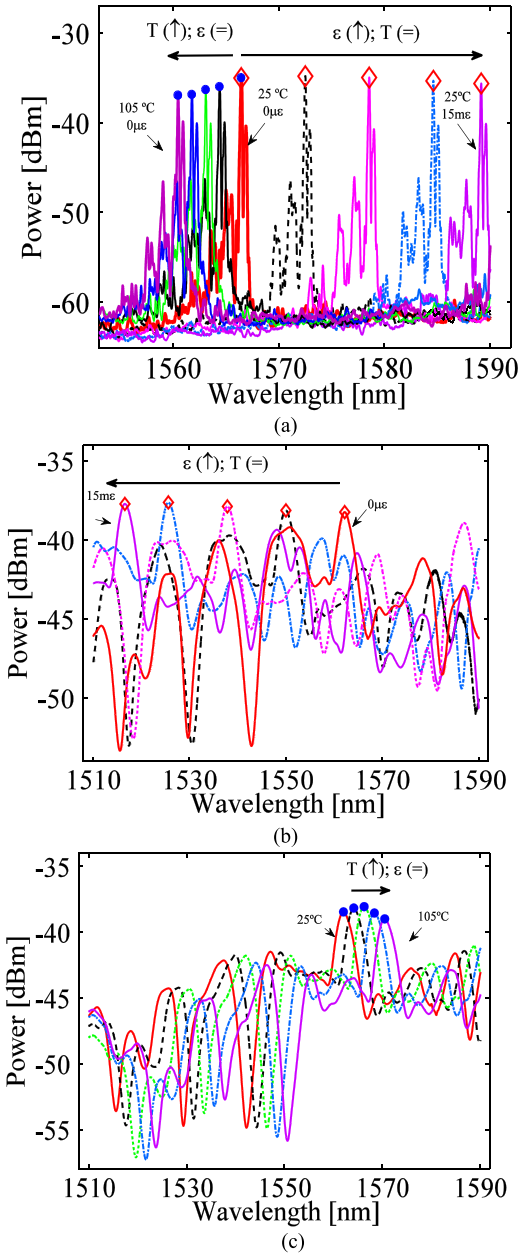

Fig. 6. (a) POFBG reflection spectra collected for the strain in the loading case. (b) and (c), SMS transmission spectra collected when the strain and temperature are increased, respectively.

hysteresis can be seen for both structure characterizations between 45 and 80 °C. The reason for such deviation could be related to the annealing process, where higher temperature or longer exposure time may be needed. By applying linear regression model to the POFBG wavelength shits, an R-square value of 0.998 is obtained for both temperature tests, where the sensitivities found are -64.6 ± 0.2 pm/°C and -64.3 ± 0.2 pm/°C for the increasing and decreasing temperature, respectively. The values are quite similar to the ones obtained for FBGs written in POFs [8], [10]. A linear regression model applied to the data points obtained for the SMS structure has produced sensitivities of 102.2 ± 0.3 pm/°C and 103.6 ± 0.3 pm/°C for the increasing and decreasing temperature, respectively, with R-square values

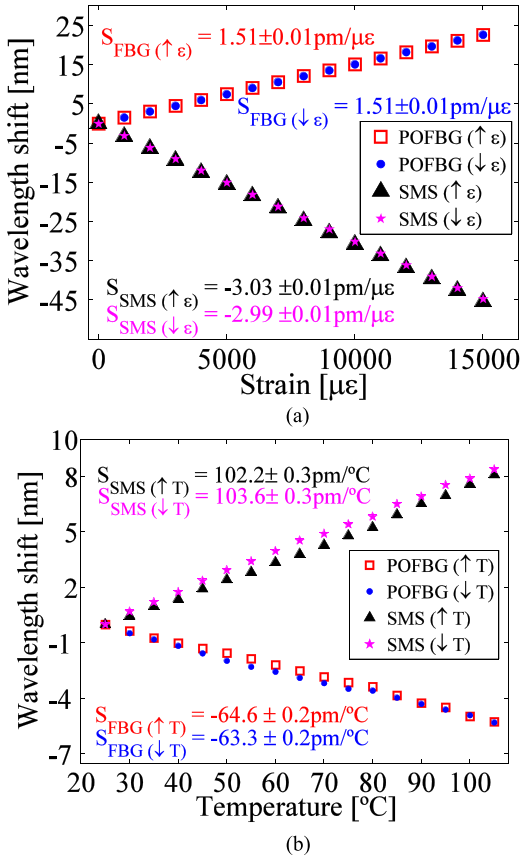

Fig. 7. (a) Wavelength shifts produced by the POFBG and SMS peak power for the strain (a) and temperature tests (b).

of 0.998 for both tests. The obtained values are three times higher than the ones found for silica fibers (i.e. [19]), but much smaller than the ones found for SMS structures based on perfluorinated [21] and partially chlorinated POFs [22]. On the other hand, our results have shown for the first time, the operation of an SMS structure based on an etched-POF in a temperature extended range, which is much higher than the ones presented in [21], [22].

It is worthy to mention that the sensitivities obtained by SMS structures are dependent on the core diameter, as well as the material (e.g. dopant) of a MMF [15].

The results concerning the effect of humidity on the wavelength stability of both POFBG and SMS structures, can be seen on Fig. 8.

The wavelength shifts observed for the POFBG and SMS structure, when the humidity was changed from 30% to 90%, are of about 70 pm and 300 pm, respectively. These wavelength shifts, although small, are higher than the expected for POF sensors based on similar polymer materials [10], [13]. Nevertheless, there are two important considerations to take into account in this test. First, the temperature errors from the climatic chamber (i.e. 0.3 °C) will impose, through the temperature sensitivities found in Fig. 7(b), errors of about 20 and 30 pm for the POFBG and SMS structure, respectively. Secondly, the climatic chamber has no water condenser, and therefore, small drops of water adhere to the surface of the etched-POF. This adhesion of water

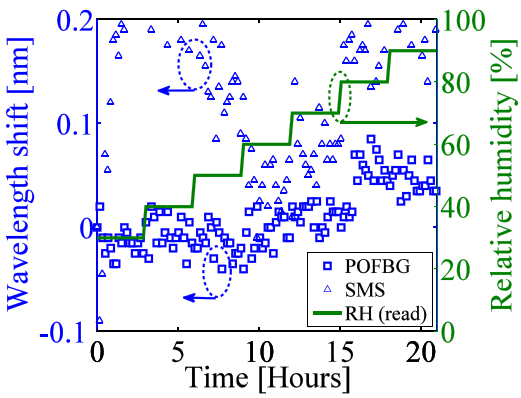

Fig. 8. Wavelength shifts produced by the POFBG and SMS peak power for the humidity test, acquired at each 10 minutes.

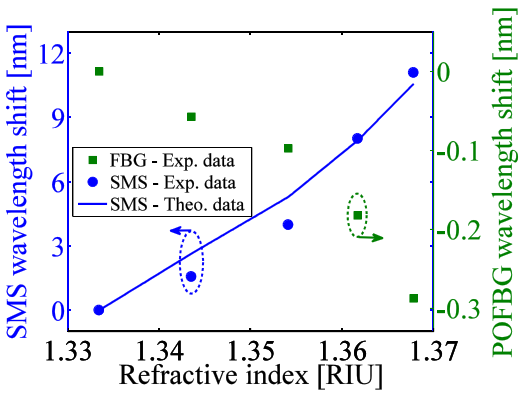

Fig. 9. Experimental and simulated SMS wavelength shifts for different external refractive index (left side); POFBG wavelength shift vs. refractive index (right side).

changes the external refractive index of the etched core fiber and thus, the wavelength shift of both POFBG and SMS structure. These measurements were realized using a box around the POF-based sensor in order to minimize such detrimental effect. When removing such protection box, the wavelength shifts were as high as 350 pm for the POFBG and 1000 pm for the SMS structure. Consequently, we cannot conclude that the observed wavelength shifts are due to the humidity change, since it can be simply due to the temperature errors, or due to the water condensation on the surface of the etched-POF that are not completely avoided with the protection box around the device.

Finally, the experimental results relative to the refractive index tests for the POFBG and SMS structure are shown on Fig. 9. The predicted SMS wavelength shift curve obtained from BPM simulations is also presented.

In this test, the reflection and transmission spectra were collected when the liquid solutions with refractive index from 1.333 to 1.368 fully cover the etched-POF. The wavelength shifts presented by the POFBG and SMS structure were inherently due to the change of the external refractive index, since there is a strong interaction of the guided modes with the external environment, contrary to what happens for step-index POF sensors based on PMMA [29], where the wavelength shift is due to the swelling and refractive index change of the PMMA material. The POFBG and SMS wavelength shifts observed for the range in study were 0.3 and 11.2 nm, revealing that the SMS structure is much more influenced by the change of the external refractive index than the POFBG. The reason is probably due to the sensing length, since the POFBG has only 4.5 mm in length, when compared with the 10 cm length of the SMS structure. On what concerns the sensitivities, a linear regression model was adjusted to the regions between [1.333−1.354] and [1.354−1.368]. The values found for the lower refractive index region were -4.49 ± 0.01 and 193.9 ± 0.01 nm/RIU, with R-square values of 0.999 and 0.994, respectively for the POFBG and SMS structure. For the higher refractive index region, sensitivity values of -13.79 ± 0.01 and 515.29 ± 0.04 nm/RIU and R-square values of 0.998 and 0.996, were obtained respectively for the POFBG and SMS structure. The presented values are intrinsically related with the diameter of the fiber used [18] and due to the refractive index of the fiber material. Nevertheless, the values found for the SMS structure in the lower refractive index region are in good agreement with the ones found in literature for unclad silica based SMS structures [18], [19].

In order to corroborate the refractive index experimental results obtained for the SMS structure, we have implemented the BPM simulation found on the numerical simulations. For that, the region around the fibers, which was previously filled with a refractive index of air ($\mathrm{n} = 1$), was now replaced by the refractive index of different solutions. The length where the 4th self-image is formed was taken for each solution and inserted in (1). The correspondent theoretical wavelength shifts are thus presented by the blue curve on Fig. 9, revealing good agreement with the experimental data.

Finally, it is worthy to mention that the sensor can be used for the simultaneous measurement of two parameters (i.e. strain and temperature or refractive index and temperature). For that, the following matrix may be applied:

$$\begin{bmatrix} x \\ T \end{bmatrix} = \begin{bmatrix} S_{x,\mathrm{FBG}} & S_{T,\mathrm{FBG}} \\ S_{x,\mathrm{SMS}} & S_{T,\mathrm{SMS}} \end{bmatrix}^{-1} \times \begin{bmatrix} \Delta\lambda_{\mathrm{FBG}} \\ \Delta\lambda_{\mathrm{SMS}} \end{bmatrix} \quad (2)$$

where x refers to the calculated strain or refractive index depending on the configuration being implemented. T defines the calculated temperature and $S_{x,\mathrm{FBG}}$ and $S_{x,\mathrm{SMS}}$ are the sensitivities of the FBG and SMS structure respectively, where the subscript "x" defines strain or refractive index (depending on the configuration). Regarding $S_{T,\mathrm{FBG}}$ and $S_{T,\mathrm{SMS}}$, they describe the temperature sensitivities of the FBG and SMS structure respectively. Finally, $\Delta\lambda_{\mathrm{FBG}}$ is the wavelength shift of the FBG, and $\Delta\lambda_{\mathrm{SMS}}$ is the wavelength shift of the SMS structure. Based on the above description, and considering a detection system with a wavelength resolution of 10 pm, the measurement errors (following reference [34]) will be 40.3 $\mu\varepsilon$ and 1.1 °C for the strain and temperature configuration, where values of 1×10^{-4} RIU and 0.2 °C will be found for the refractive index and temperature configuration (for both refractive index regions).

V. Conclusion

In this work a new fiber optic sensor based on a POFBG and an SMS structure is presented. The multimode fiber is based

on an etched-POF whose core is made by COP material. The results have shown the capability to measure strain and temperature with limits of 1.5% and 105 °C, respectively. Additionally, the ability to detect refractive index with the POF based SMS structure is shown for the first time. The obtained sensitivities are validated theoretically and similar to the ones shown in literature. Nevertheless, the low water absorption characteristics offered by the COP material reveal that the sensor is weakly influenced by the external humidity. Moreover, the use of both fiber structures (POFBG and SMS), can be employed on a multiparameter scheme.

REFERENCES

[1] A. Cusano, A. Cutolo, and J. Albert, *Fiber Bragg Grating Sensors: Recent Advancements, Industrial Applications and Market Exploitation*, 1st ed. Sharjah, UAE: Bentham Science Publishers, 2011.

[2] K. Minami, "Optical Plastics," in *Handbook of Plastic Optics*, 2nd ed., S. Bäumer, Ed. Weinheim, Germany: Wiley, 2010, pp. 123–196.

[3] J. Huang *et al.*, "Polymer optical fiber for large strain measurement based on multimode interference," *Opt. Lett.*, vol. 37, no. 20, pp. 4308–4310, 2012.

[4] Z. Xiong, G. D. Peng, B. Wu, and P. L. Chu, "Highly tunable Bragg gratings in single-mode polymer optical fibers," *IEEE Photon. Technol. Lett.*, vol. 11, no. 3, pp. 352–354, Mar. 1999.

[5] G. Emiliyanov *et al.*, "Localized biosensing with topas microstructured polymer optical fiber," *Opt. Lett.*, vol. 32, no. 5, pp. 460–462, 2007.

[6] W. Zhang, D. J. Webb, and G.-D. Peng, "Investigation into time response of polymer fiber bragg grating based humidity sensors," *J. Light. Technol.*, vol. 30, no. 8, pp. 1090–1096, 2012.

[7] W. Zhang and D. J. Webb, "Humidity responsivity of poly(methyl methacrylate)-based optical fiber Bragg grating sensors," *Opt. Lett.*, vol. 39, no. 10, pp. 3026–3029, 2014.

[8] R. Oliveira, L. Bilro, J. Heidarialamdarloo, and R. Nogueira, "Fabrication and characterization of polymer fiber Bragg gratings inscribed with KrF UV laser," in *Proc. Int. Conf. Plastic Opt. Fibers*, 2015, pp. 371–375.

[9] A. Fasano *et al.*, "Fabrication and characterization of polycarbonate microstructured polymer optical fibers for high-temperature-resistant fiber Bragg grating strain sensors," *Opt. Mater. Exp.*, vol. 6, no. 2, pp. 649–659, 2016.

[10] W. Yuan *et al.*, "Humidity insensitive TOPAS polymer fiber Bragg grating sensor," *Opt. Express*, vol. 19, no. 20, pp. 19731–19739, Sep. 2011.

[11] S. G. Leon-Saval, R. Lwin, and A. Argyros, "Multicore composite single-mode polymer fibre," *Opt. Express*, vol. 20, no. 1, pp. 141–148, 2012.

[12] Asahi Glass Co. Ltd., "Amorphous fluoropolymer CYTOP," Asahi Glass Co. Ltd., Tokyo, Japan, 2009.

[13] G. Woyessa, A. Fasano, A. Stefani, C. Markos, H. K. Rasmussen, and O. Bang, "Single mode step-index polymer optical fiber for humidity insensitive high temperature fiber Bragg grating sensors," *Opt. Express*, vol. 24, no. 2, pp. 1253–1260, 2016.

[14] G. Woyessa *et al.*, "Humidity insensitive step-index polymer optical fibre Bragg grating sensors," in *Proc. 24th Int. Conf. Opt. Fibre Sensors*, 2015, vol. 9634, Art. No. 96342L.

[15] S. M. Tripathi, A. Kumar, R. K. Varshney, Y. B. P. Kumar, E. Marin, and J.-P. Meunier, "Strain and temperature sensing characteristics of single-mode–multimode–single-mode structures," *J. Light. Technol.*, vol. 27, no. 13, pp. 2348–2356, 2009.

[16] S. Silva *et al.*, "Ultrahigh-sensitivity temperature fiber sensor based on multimode interference," *Appl. Opt.*, vol. 51, no. 16, pp. 3236–3242, 2012.

[17] J. E. Antonio-Lopez, J. J. Sanchez-Mondragon, P. LiKamWa, and D. A. May-Arrioja, "Fiber-optic sensor for liquid level measurement," *Opt. Lett.*, vol. 36, no. 17, pp. 3425–3427, 2011.

[18] Q. Wu, Y. Semenova, P. Wang, and G. Farrell, "High sensitivity SMS fiber structure based refractometer—Analysis and experiment," *Opt. Express*, vol. 19, no. 9, pp. 7937–7944, 2011.

[19] R. Oliveira, J. H. Osório, S. Aristilde, L. Bilro, R. N. Nogueira, and C. M. B. Cordeiro, "Simultaneous measurement of strain, temperature and refractive index based on multimode interference, fiber tapering and fiber Bragg gratings," *Meas. Sci. Technol.*, vol. 27, no. 7, 2016, Art. no. 75107.

[20] M. Shao *et al.*, "Refractive index measurement based on fiber Bragg grating connected with a multimode fiber core," *Opt. Commun.*, vol. 351, pp. 70–74, 2015.

[21] G. Numata, N. Hayashi, M. Tabaru, Y. Mizuno, and K. Nakamura, "Ultrasensitive strain and temperature sensing based on modal interference in perfluorinated polymer optical fibers," *IEEE Photon. J.*, vol. 6, no. 5, Oct. 2014, Art. no. 6802306.

[22] G. Numata, N. Hayashi, M. Tabaru, Y. Mizuno, and K. Nakamura, "Strain and temperature sensing based on multimode interference in partially chlorinated polymer optical fiber," *IEICE Electron. Express*, vol. 12, no. 2, pp. 20141173–2014117, Jan. 2015.

[23] M. S. Ferreira, J. Bierlich, M. Becker, K. Schuster, J. L. Santos, and O. Frazão, "Ultra-high sensitive strain sensor based on post-processed optical fiber Bragg grating," *Fibers*, vol. 2, pp. 142–149, 2014.

[24] W. Liang, Y. Huang, Y. Xu, R. K. Lee, and A. Yariv, "Highly sensitive fiber bragg grating refractive index sensors," *Appl. Phys. Lett.*, vol. 86, no. 15, 2005, Art. no. 151122.

[25] R. Oliveira, C. A. F. Marques, L. Bilro, and R. N. Nogueira, "Production and characterization of Bragg gratings in polymer optical fibers for sensors and optical communications," in *Proc. Int. Conf. Opt. Fiber Sensors*, 2014, vol. 23, Art. no. 915794.

[26] R. Oliveira, L. Bilro, and R. Nogueira, "Bragg gratings in a few mode microstructured polymer optical fiber in less than 30 seconds," *Opt. Express*, vol. 23, no. 8, pp. 10181–10187, 2015.

[27] L. B. Soldano and E. C. M. Pennings, "Optical multi-mode interference devices based on self-imaging: principles and applications," *J. Light. Technol.*, vol. 13, no. 4, pp. 615–627, 1995.

[28] R. Selvas *et al.*, "Wavelength tuning of fiber lasers using multimode interference effects," *Opt. Express*, vol. 13, no. 23, pp. 9439–9445, 2005.

[29] R. Ferreira, L. Bilro, C. Marques, R. Oliveira, and R. Nogueira, "Refractive index and viscosity: Dual sensing with plastic fibre gratings," in *Proc. Int. Conf. Opt. Fiber Sensors*, 2014, vol. 23, Art. no. 915793.

[30] [Online]. Available: http://www.zeonex.com. Accessed on: 10 May 2016.

[31] R. Oliveira *et al.*, "Bragg gratings inscription in highly birefringent microstructured POFs," *Photon. Technol. Lett.*, vol. 28, no. 6, pp. 621–624, 2016.

[32] E. Adhesives, "The adhesive sourcebook," 2015, vol. 9.

[33] Y. Liu and L. Wei, "Low-cost high-sensitivity strain and temperature sensing using graded-index multimode fibers," *Appl. Opt.*, vol. 46, no. 13, pp. 2516–2519, 2007.

[34] D.-P. Zhou, L. Wei, W.-K. Liu, Y. Liu, and J. W. Y. Lit, "Simultaneous measurement for strain and temperature using fiber bragg gratings and multimode fibers," *Appl. Opt.*, vol. 47, no. 10, pp. 1668–1672, 2008.

Authors' biographies not available at the time of publication.